Supporting Information

Supporting Information Corrected September 12, 2016
Kopp et al. 10.1073/pnas.1517056113

Sensitivity Tests for Reconstruction

We consider five alternative empirical calibrations of the hyperparameters $\boldsymbol{\Theta} = \{\sigma_g, \sigma_l, \sigma_m, \sigma_w, \sigma_0, \sigma_{g0}, \tau_g, \tau_m, \lambda_l, \lambda_m\}$ (Dataset S1, c, and Fig. S3). (*i*) For prior $ML_{2,2}$, $\boldsymbol{\Theta}$ is empirically calibrated through a hybrid global simulated annealing/local sequential quadratic programming optimization to find the hyperparameters that maximize the likelihood of the model conditional upon the observations. (*ii*) Prior $ML_{2,1}$ is similar to prior $ML_{2,2}$, but with the constraint that $\tau_m = \tau_g$, i.e., that there is one timescale hyperparameter for the nonlinear terms. (*iii*) Prior $ML_{1,1}$ is similar to prior $ML_{2,2}$, but with the constraints that $\tau_m = \tau_g$ and $\sigma_m = \sigma_g$, i.e., that there is one timescale hyperparameter and one amplitude hyperparameter for the nonlinear terms. (*iv*) For prior NC, σ_g and τ_g are optimized to maximize the likelihood of a GP model fit to the curve derived from the detrended North Carolina RSL reconstruction. The remaining hyperparameters are then empirically optimized to maximize the likelihood of the model conditional upon the observations. (*v*) For prior Gr, σ_g and τ_g are optimized to maximize the likelihood of a GP model fit to the ref. 20 GSL hindcast. The remaining hyperparameters are then empirically optimized to maximize the likelihood of the model conditional upon the observations.

In all cases, the parameters were optimized conditional only upon observations with 2σ age uncertainties of less than ± 50 years. In order to ensure that the optimization process does not confuse the interpretations of the terms reflecting the processes of interest and the white-noise term, we optimized under the constraint that τ_g and $\tau_m > 100$ y. To ensure that this is a reasonable constraint, we also tested a model in which the amplitude of the global term, σ_g, was set equal to zero; thus, in this model, all observations were interpreted as reflecting regional changes. Without the inclusion of the global term, the optimal value of τ_m is 123 y, consistent with the constraint.

From an interpretive perspective, the main difference among the calibrated prior is the timescale of GSL variability τ_g (Dataset S1, c). In priors $ML_{2,1}$ and $ML_{1,1}$, this timescale is ~ 100 y, whereas, for $ML_{2,2}$, it is ~2,000 y, yielding an overly smooth GSL curve; other priors have intermediate timescales. Shorter timescales lead a greater proportion of centennial-scale variability to be attributed to GSL. Although $ML_{2,2}$ has the highest marginal likelihood, we focus on $ML_{2,1}$ in presenting results, as inspection of within-20th century rate estimates for $ML_{2,2}$ suggests oversmoothing. Prior estimates of rates and variability are shown in Dataset S1, d.

We also consider the application of the model with the $ML_{2,1}$ before different subsets of data (Dataset S1, f). The decline in GSL between 1000 CE and 1400 CE is robust to the removal of North Atlantic data ($P = 0.91$ in subset -NAtlantic+GSL) and to the consideration only of data from the Atlantic and the Mediterranean ($P = 1.00$ in subset +AtlanticMediterranean+GSL). It is, however, not robust to the consideration only of data from South America ($P = 0.48$ in subset +SAmerica+GSL) or only of data outside the Atlantic and Mediterranean ($P = 0.25$ in subset -AtlanticMediterranean+GSL).

To assess the impact of the exogenous ref. 12 GSL curve for the 20th century, we consider each subset of data with and without the inclusion of this curve (indicated in Dataset S1, f by +GSL and -GSL). Twentieth century rates have broader errors without the exogenous 20th century curve but are in general agreement with that curve (e.g., +All+GSL: 1.38 ± 0.15 mm/y; +All-GSL: 1.31 ± 0.33 mm/y).

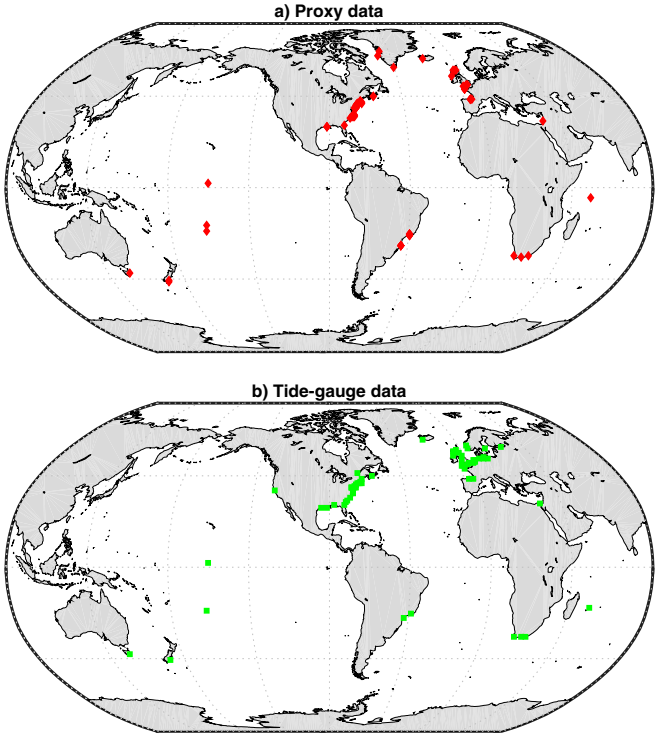

Fig. S1. Locations of sites with (*A*) proxy data and (*B*) tide-gauge data included in the analysis.

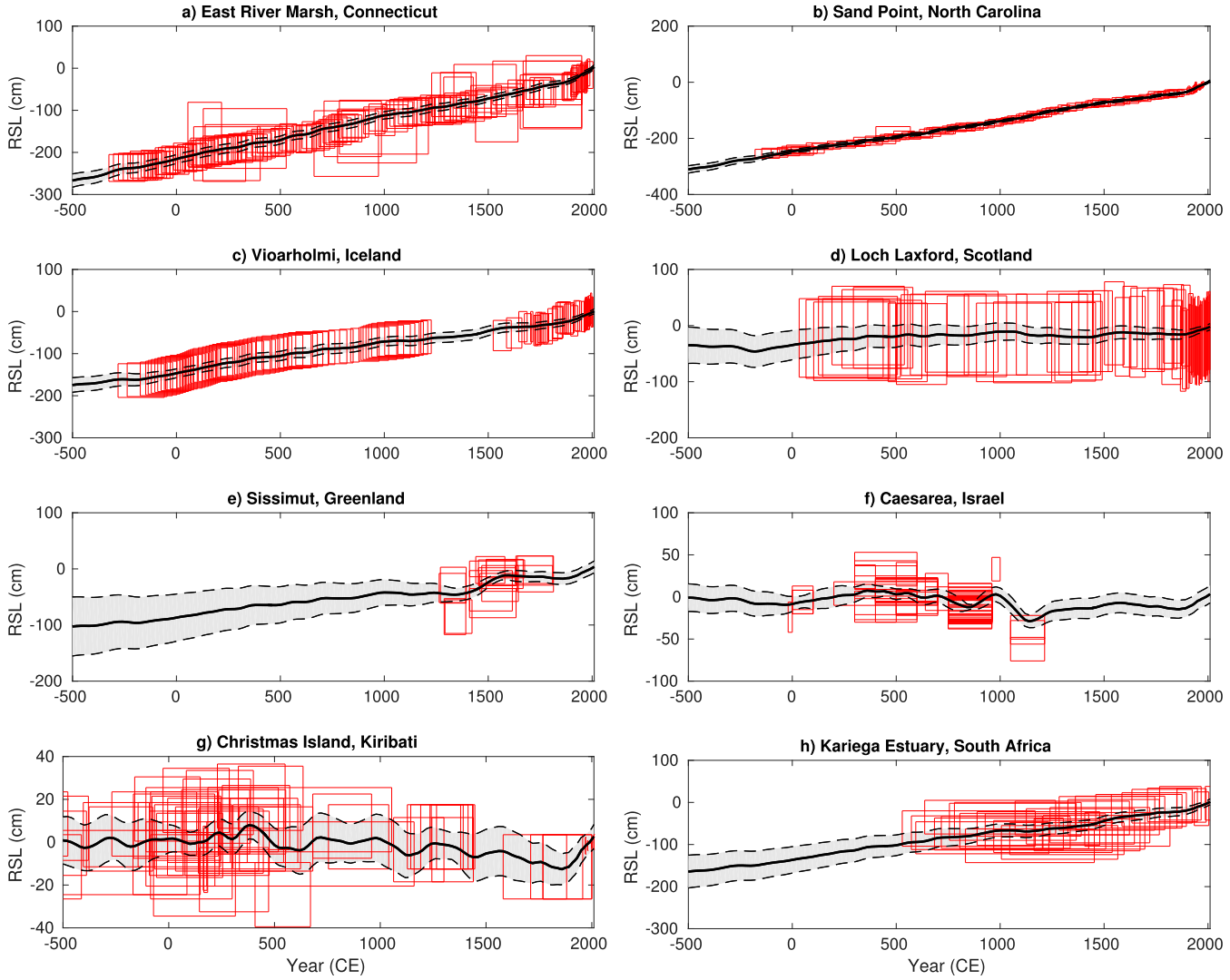

Fig. S2. Model fits under prior $ML_{2,1}$ at eight illustrative sites: (*A*) East River Marsh, CT; (*B*) Sand Point, NC, (*C*) Vioarholmi, Iceland, (*D*) Loch Laxford, Scotland, (*E*) Sissimut, Greenland, (*F*) Caesarea, Israel, (*G*) Christmas Island, Kiribati, and (*H*) Kariega Estuary, South Africa. (Note that the model fit at each site is informed by all observations, not just those at the illustrated site.) Red boxes show all data points within 0.1 degrees of the centroid of the named site. Errors are $\pm 2\sigma$.

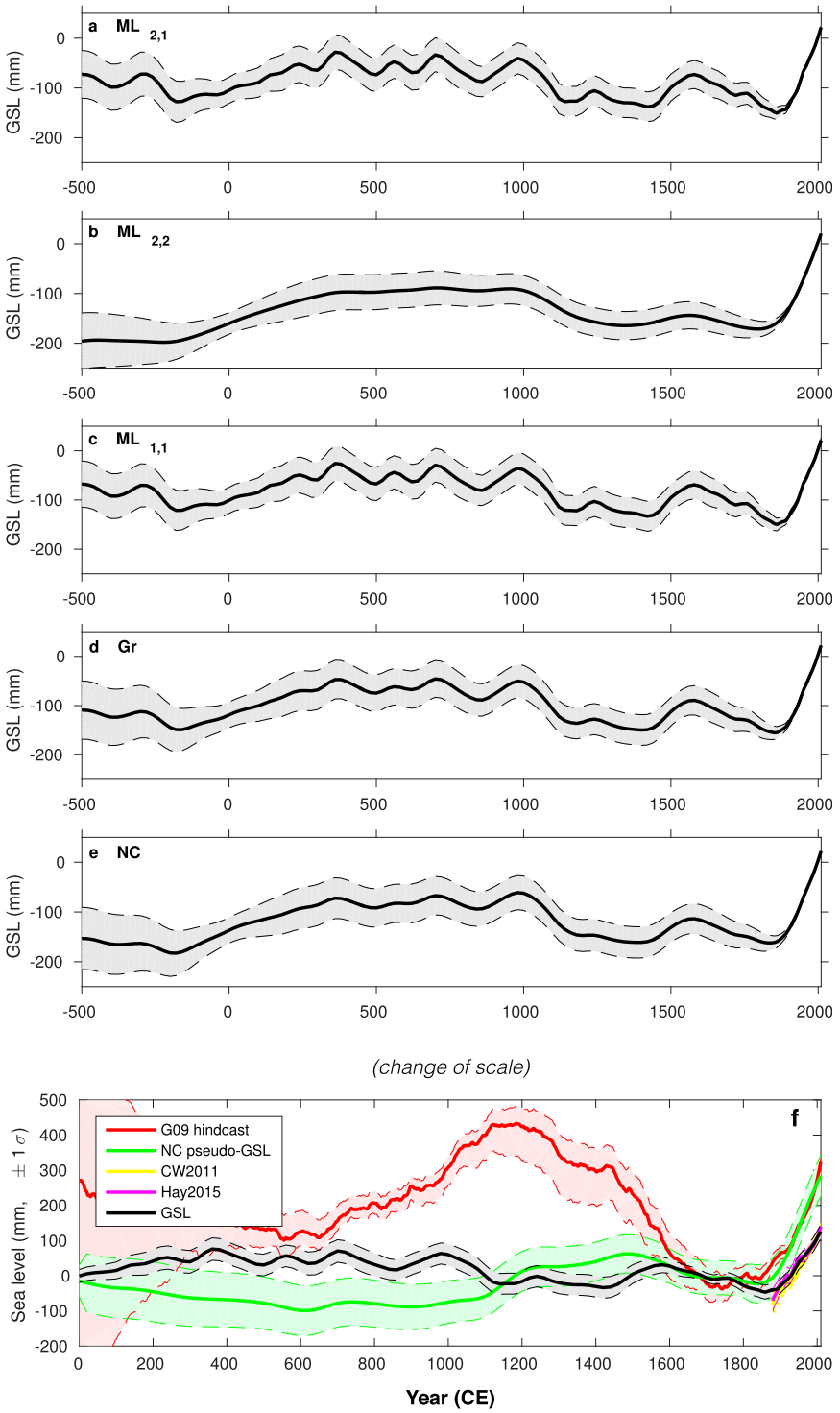

Fig. S3. (*A*–*E*) GSL estimates under priors (*A*) $ML_{2,1}$, (*B*) $ML_{2,2}$, (*C*) $ML_{1,1}$, (*D*) Gr, and (*E*) NC. (*F*) GSL reconstruction under prior $ML_{2,1}$ (black) compared with the hindcast of ref. 20 (G09 hindcast; red), a curve derived from the North Carolina RSL curve by detrending and the addition of ± 10 mm (2σ) errors after ref. 5 (NC pseudo-GSL; green), and the 19th–20th century GMSL reconstructions of ref. 12 (Hay2015; magenta) and ref. 106 (CW2011; yellow). Multicentury records are aligned relative to the 1600–1800 CE average; 19th–20th century reconstructions are aligned to match our GSL reconstruction in 2000 CE. Errors are $\pm 1\sigma$.

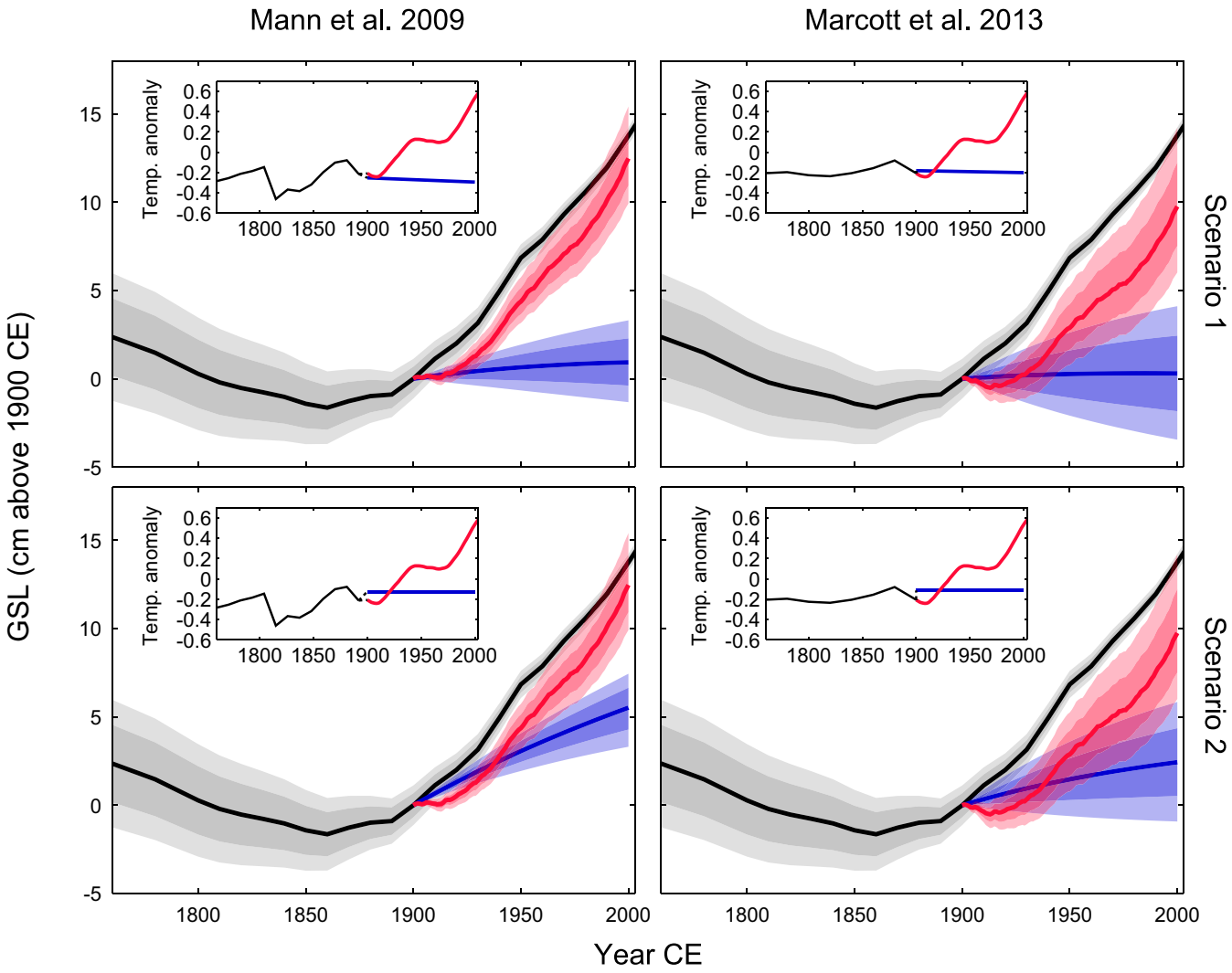

Fig. S4. Counterfactual hindcasts of global mean sea-level rise in the absence of anthropogenic warming. Each row assumes a different counterfactual temperature scenario (see *Materials and Methods*), while each column represents model calibration to a different temperature reconstruction (*Inset*). In the temperature *Insets*, the black lines represent the original temperature reconstruction to 1900, the red line represents the HadCRUT4 temperature reconstruction for the 20th century, and the blue line represents the counterfactual scenario. In the main plots, the red and blue curves correspond, respectively, to the HadCRUT4 and counterfactual temperature scenarios. The difference between them can be interpreted as the anthropogenic GSL rise. Heavy shading, 67% credible; light shading, 90% credible.

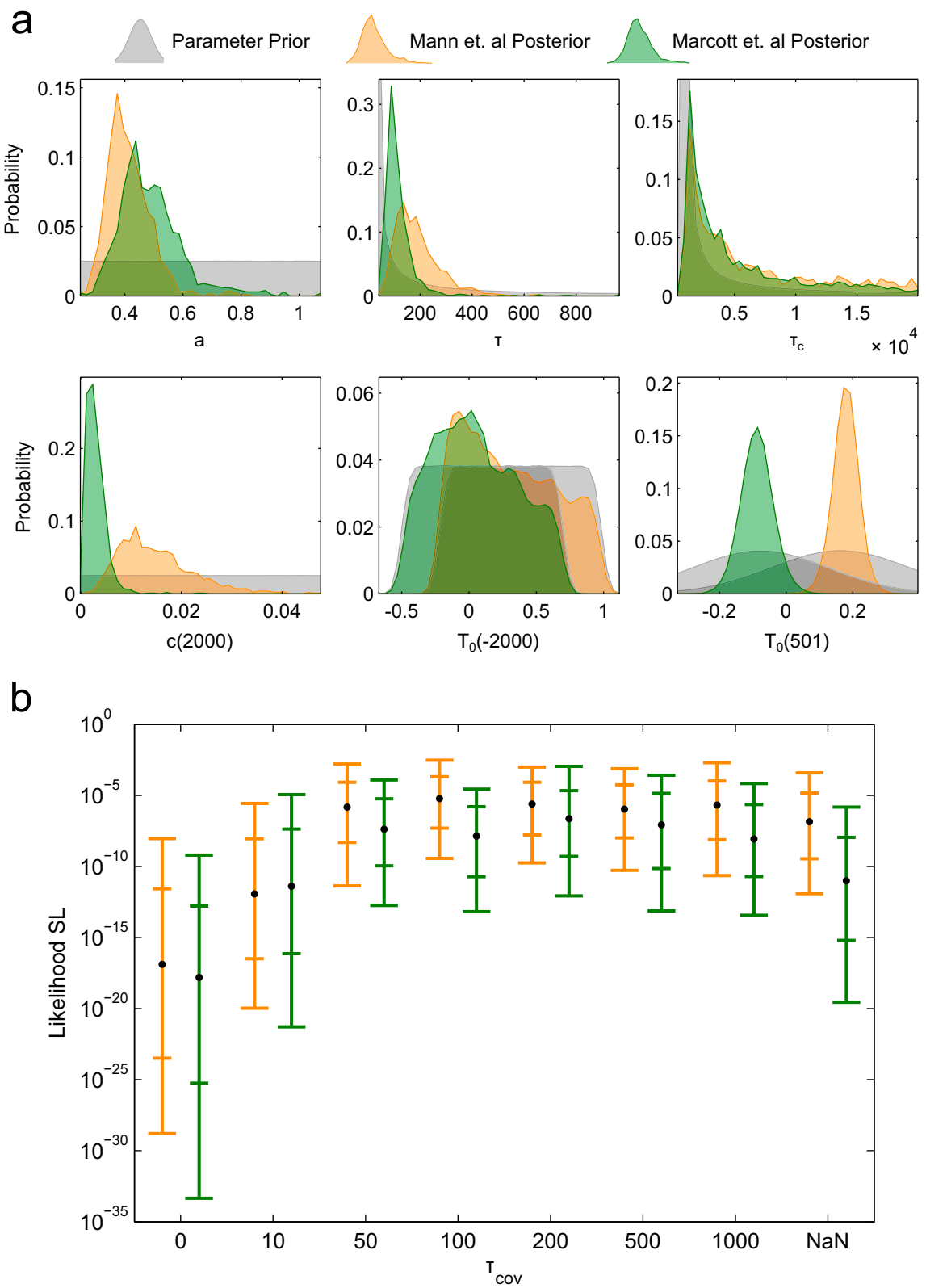

Fig. S5. (*A*) Probability distributions of semiempirical model parameters. Prior distributions (gray) are not shown in full where scaling axes to display them would render posteriors obscure. (*B*) Likelihood of different values of τ_{cov}. Black dots show likelihoods across all semiempirical projections, and the bars show the 5th/17th/83rd/95th percentile conditional likelihoods for individual semiempirical projections. A value of $\tau_{cov} = 100$ y is used in the analysis. Orange [green] represents calibration with the Mann et al. (1) [Marcott et al. (2)] temperature curve.

Dataset S1. (a) A summary of the sites included in the Common Era database, (b) a summary of the tide gauges incorporated into the metaanalysis, (c) hyperparameters of the different priors for the empirical hierarchical model, (d) prior estimates of GSL rates and amplitude of variability under different priors, (e) posterior estimates of GSL rates and amplitude of variability under different priors, (f) GSL rates under different data subsets, (g) RSL rates at different sites, (h) semiempirical estimates of the probability that the observed GSL rise exceeds counterfactual projections, (i) semiempirical GSL projections, and (j) the distribution of semiempirical model parameters

Dataset S1

Dataset S2. The full Common Era RSL reconstruction database

Dataset S2

Dataset S3. Time series and covariance matrices of GSL under the five different priors

Dataset S3